Electronic Supplementary Material (ESI) for Physical Chemistry Chemical Physics.

Supplementary Information for:

Spin rectification by orbital polarization in Bi-bilayer nanoribbons

Kyung-Hwan Jin[a,b] *and Seung-Hoon Jhi**[a]

[a]Department of Physics, Pohang University of Science and Technology, Pohang 790-784, Republic of Korea

[b]Department of Materials Science and Engineering, University of Utah, Salt Lake City, UT 84112, United States

Correspondence and requests for materials should be addressed to Seung-Hoon Jhi (jhish@postech.ac.kr)

1. Band structure of armchair-edged Bi (111) bilayer nanoribbon

In a Bi (111) bilayer, two-layer Bi atoms form the honeycomb lattice. The in-plane lattice constant and the inter-layer distance are calculated to be 4.340 Å and 1.735 Å, respectively. To investigate the edge properties of the BNRs, we study two representative model systems: zigzag-edged and armchair-edged nanoribbon.

Edge states of ABNRs are also sensitive to the chemical passivation. Fig. S1 (a) and (b) shows calculated band structures of 28-ABNR without or with hydrogen-passivation. Non-passivation edge has two Dirac points in the band gap at Γ and π points. But topologically-protected edge states appear at Γ point regardless of the passivation.

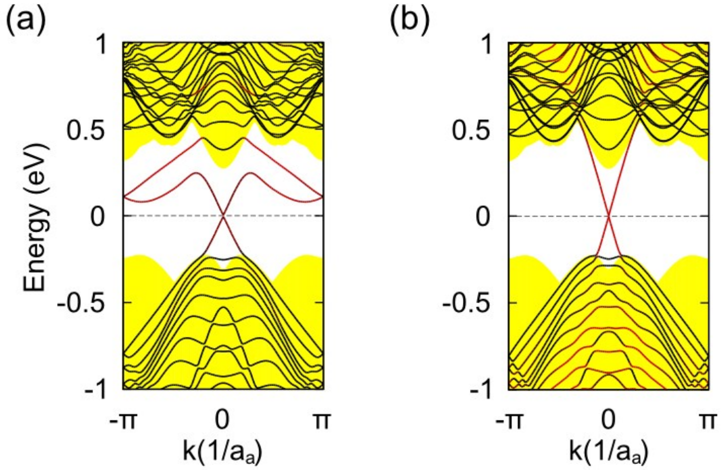

Fig. S1 Band structure of armchair-edge Bi nanoribbon. Calculated band structures of 28-ABNR (a) without edge passivation and (b) with hydrogen passivation. The shaded (yellow) region denotes the bulk band structure of 2D Bi (111) bilayer projected into 1D Brillouin zone of the nanoribbon.

2. The energy band-gap for various width and chemical-passivation nanoribbons

Fully hydrogen-passivated Bi nanoribbon shows the linear band dispersion at the Γ point if the nanoribbon is wide enough so that coupling of the edge states is negligible. For the linear dispersion ($E=v_fk$), the density of state $g(E)$ is then a constant ($\propto 1/v_f$) [Fig. S2]. When the nanoribbon is narrow, the band-gap is opened by the inter-edge interaction. Calculated band gaps of Bi nanoribbons decrease exponentially with increasing nanoribbon width. We found that the passivation by other molecular species like NO_2 or –OH works the same as the hydrogen passivation.

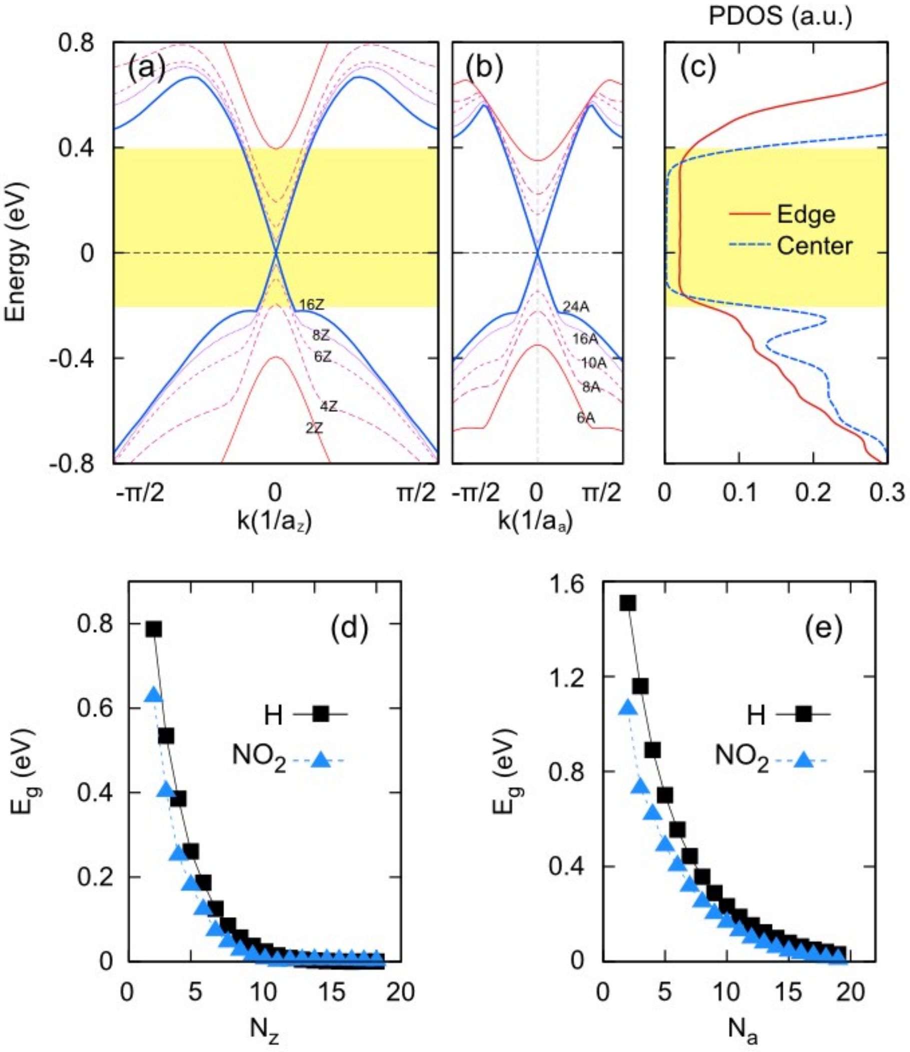

Fig. S2 Width dependence of nanoribbon band structures. Calculated band structures of (a) zigzag- and (b) armchair-edged BNRs as the nanoribbon width is changed. We observe finite band gaps for narrow BNRs but sharp Dirac-cone bands for wide BNRs (16-ZBNR and 24-ABNR as denoted by 16Z and 24A, respectively). (c) Calculated projected density of states (PDOS) into the edge (in red) or the center atom (in dashed blue) in 16-ZBNR. We observe that finite (constant) PDOS near the Fermi level comes from the linear-band edge states. (d) and (e), Calculated band gaps of BNRs with zigzag-edge and armchair-edge structures, respectively. The coupling between the edge states in BNRs opens a band gap that decreases exponentially upon increasing width. The gap shows weak dependence on passivating chemicals, which affect the localization of the edge states.

3. Hydrogen-passivation-coverage dependence of the edge states in BNR

The hydrogen passivation of the edges modifies dramatically the Fermi velocity of the Dirac states as reflected on the band slope and the Dirac-cone position. We studied the coverage dependence of the edge states by changing the ratio of dangling bonds and hydrogen passivation to reveal the shift in the Dirac cone position. As hydrogen saturates the dangling bonds of edge Bi atoms, the edge states are stabilized in energy and the conduction band shifts down to merge into the Dirac band.

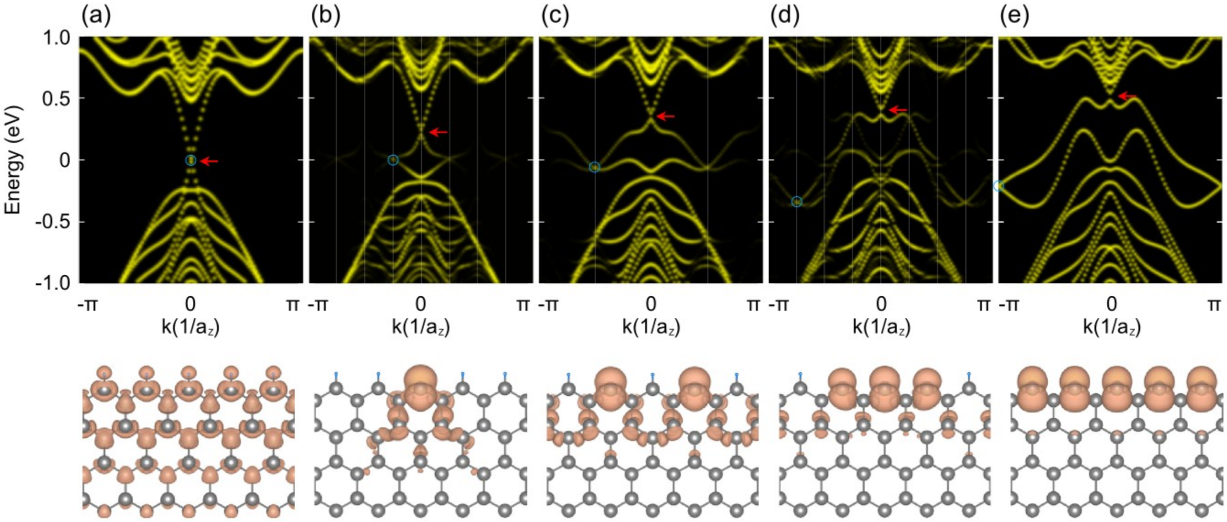

Fig. S3 Coverage dependence of the edge states for hydrogen passivation. Calculated band structures of 10-ZBNR with decreasing coverage of hydrogen passivation of edge atoms [from (a) to (e)]. Lower panels show the squared wave-function of the edge state at the Dirac point (marked by a circle in the band structure in the upper panel). Part of BNRs with the axis along the horizontal direction is shown with Bi atoms in large gray circles and hydrogen atoms at the edge (top side) in small dots. As the dangling bonds are passivated by hydrogen gradually [from (e) to (a)], the conduction band minimum (marked by the red arrow) is lowered to develop a

Dirac cone at Γ point. The Dirac cone at X point shifts down in energy and disappears in the energy range shown. The states at the Dirac point are highly localized at the edge without edge passivation but, with edge passivation, become more dispersed into the BNR center having a tail of around 10Å.

4. The spin texture of the edge states

The spin texture of topological edge states can be modified by the edge passivation. Figure S4 shows detailed spin texture of the conduction and valence band states of asymmetric 20-ZBNR in Fig. 2(c). We see that the spin of the states is in the *xz*-plane, perpendicular to the momentum (y-direction). Non-passivated edge has the in-plane (x-direction) spin component is dominant near the Dirac point. However, the spin direction of edge state continuously rotate as the k-point goes away from the Dirac point. With H passivation, the main spin component is out-of-plane (z-direction) component near the Γ point. Thus, the spin direction is warping along the Dirac state with different momenta.

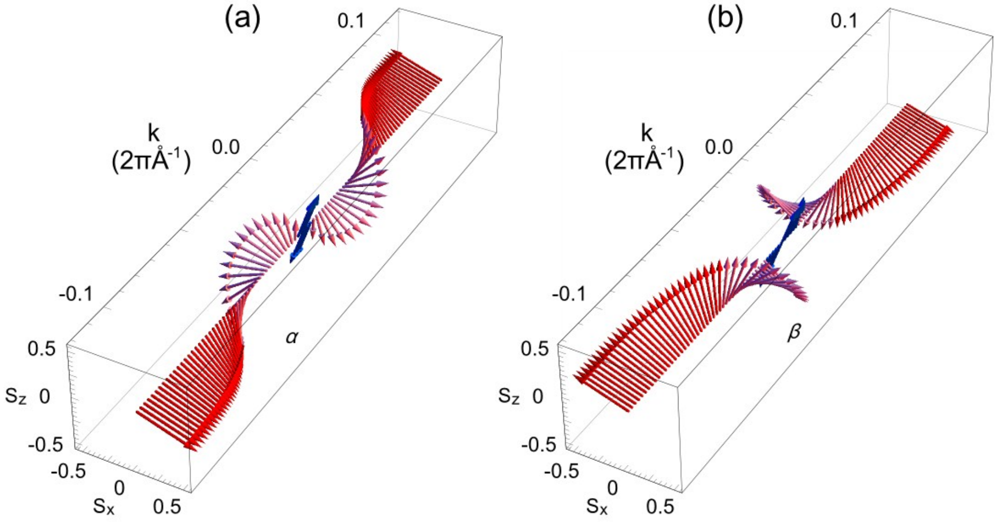

Fig. S4 The spin texture of edge states. The spin direction of the states (a) in the valence band (α) and (b) in the conduction (β) band of 20-ZBNR with asymmetric passivation shown in Fig. 2c. The spins at opposite edges rotates by about ~90°.

5. Spin rotation under electric fields

The electric field can control the spin of the helical edge states of ZBNR as it polarizes the atomic orbitals. The spin rotates counterclockwise in the *xz*-plane as the strength of the electric field is increased. The rotation turns clockwise when the electric field is reversed in direction (Fig. S5). If we apply the electric fields in the opposite directions at the edges, say one in the "up" dicretion and the other in the "down" direction, the spin of the helical states at the edges can be aligned in the same direction by tuning the electric field strength.

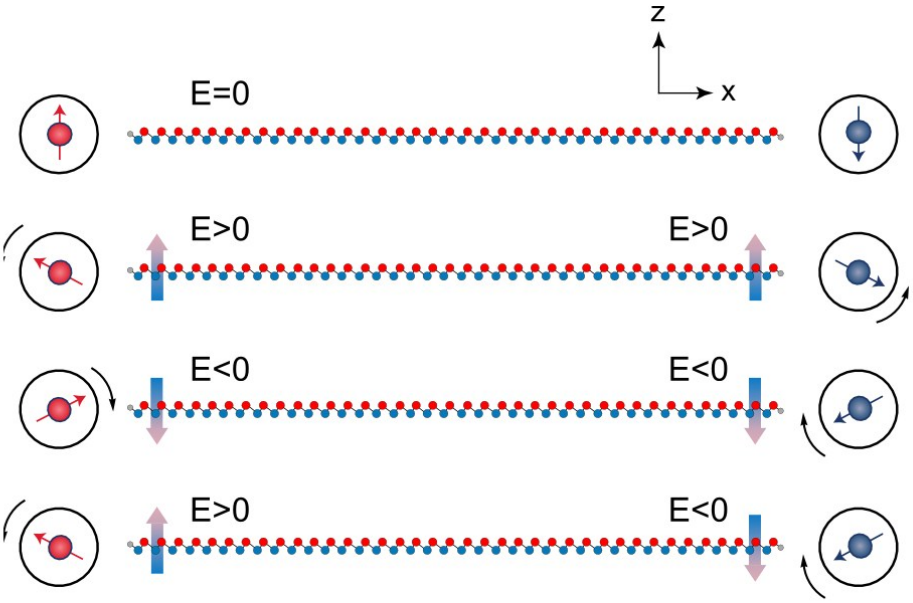

Fig. S5 The spin of electron of the edge states under electric fields. For the electric field in the "up" ("down") direction, the spin rotates counterclockwise (clockwise). As such, the spin at the two edges can be aligned in the same direction by applying the electric fields in the opposite directions and tuning the field strength.

6. The band structure of curved ZBNR

We investigated the effect of structural deformation on the electronic structure of ZBNRs. In particular, we studied the bending of 38-ZBNR transverse to the ribbon axis. Calculated band structures are shown in Fig. S6 (a-d) with increasing bending angles. As the bending angle (θ) is increased, new valence states originated from the bent regions appear inside the bulk gap. The bending does not change the topological property of the edge states (a-d). The helical edge states develop at Γ point and are localized at the edges. Fig. S6 (e) and (f) show the real-space charge distributions of the edge states for flat and curved 38-ZBNR, respectively. For the flat case, two Dirac states are localized at the edges, one at the left and the other at the right edge. Curved ZBNR also have two Dirac states localized at the edges and, in addition, a new state localized at the bent region.

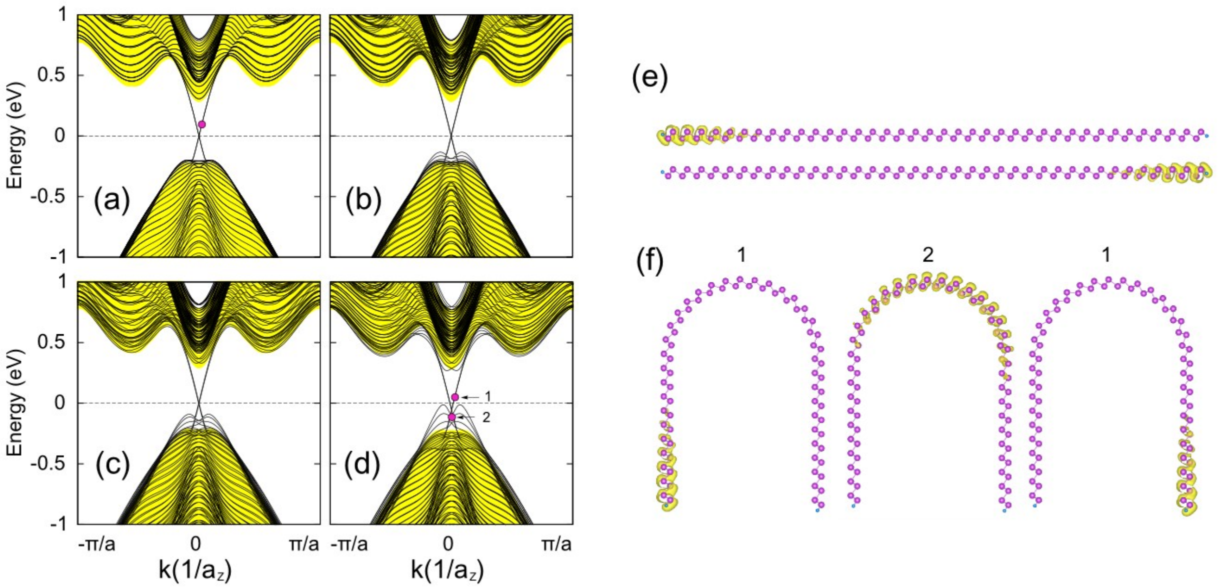

Fig. S6 Band structure of curved ZBNR and charge distribution. Calculated band structures of curved 38-ZBNR for bending angle of (a) 0˚, (b) 18˚, (c) 45˚, and (d) 90˚. The shaded regions are the bulk states projected into 1D Brillouin zone. Side views of flat (e) and curbed ZBNR (f) and the squared wave-function (in yellow) of the edge states marked by red dots in (a) (θ= 0˚) and (d) (θ=90˚). Bi in purple circles and H in small blue dots.